Diluted magnetic semiconductors based on $Sb_{2-x}V_xTe_3$ ($0.01 \leqslant x \leqslant 0.03$)

Jeffrey S. Dyck,[1] Pavel Hájek,[2] Petr Lošťák,[2] and Ctirad Uher[1,*]
[1]*Department of Physics, University of Michigan, Ann Arbor, Michigan 48109*
[2]*Department of General and Inorganic Chemistry, Faculty of Chemical Technology, University of Pardubice, Čs. Legií 565, 532 10 Pardubice, Czech Republic*
(Received 9 October 2001; published 8 March 2002)

We report on a diluted magnetic semiconductor based on the Sb_2Te_3 tetradymite structure doped with very low concentrations of vanadium (1–3 at. %). The anomalous transport behavior and robust magnetic hysteresis loops observed in magnetotransport and magnetic measurements are experimental manifestations of the ferromagnetic state in these materials. The p-d exchange between holes and vanadium $3d$ spins is estimated from the behavior of the magnetoresistance. A Curie temperature of at least 22 K is observed for $Sb_{1.97}V_{0.03}Te_3$. This discovery offers possibilities for exploring magnetic properties of other tetradymite structure semiconductors doped with a wide range of $3d$ transition metals.

DOI: 10.1103/PhysRevB.65.115212 PACS number(s): 75.50.Pp, 72.80.Jc, 75.60.Ej

I. INTRODUCTION

Since the first studies of the coexistence of ferromagnetism and semiconducting properties in Eu chalcogenides and semiconducting spinels,[1] the rich interplay between magnetic cooperative phenomena and semiconducting properties has received considerable attention. Diluted magnetic semiconductors (DMS's), which display this behavior, are classical semiconductors where a controlled fraction of the nonmagnetic cation is substituted by transition-metal or rare-earth ions. The most extensively studied DMS's are based on the II-VI or III-V ternary compounds where Mn^{2+} ions serve as the magnetic impurity,[2–5] and ferromagnetic interaction among localized Mn spins has been seen in thin films of low-temperature molecular beam epitaxy (MBE)-grown p-type InAs and GaAs.[3–5] These DMS's have tetrahedral bonds and crystallize in either the zinc-blende or wurtzite structure, and their magnetic properties are intimately tied to the presence of the manganese ions. Our diluted magnetic semiconductor is based on Sb_2Te_3 and differs from the existing DMS's in two important respects: it crystallizes with an anisotropic tetradymite-type structure with atoms in an octahedral coordination; and the magnetic ion is not manganese but vanadium.

The parent crystal, Sb_2Te_3, is a narrow-band-gap semiconductor with tetradymite structure (space group $R\bar{3}m - D_{3d}^5$) that belongs to the family of compounds with the form $A_2^{\mathrm{V}}B_3^{\mathrm{VI}}$ (where A=Bi, Sb and B=Se, Te). The crystal lattice of Sb_2Te_3 (see Fig. 1) consists of repeated groups of atomic layers, $Te^{(2)}$-Sb-$Te^{(1)}$-Sb-$Te^{(2)}$, oriented perpendicular to the trigonal c axis, with primarily ionic and covalent bonding within the layers ($Te^{(1)}$-Sb and Sb-$Te^{(2)}$), and van der Waals bonding between the Te sheets forming the double layers ($Te^{(2)}$-$Te^{(2)}$).[6] This interesting crystal structure results in anisotropic transport[7] and optical properties[8] and this class of materials forms the backbone of the present-day thermoelectric cooling devices.[7] Sb_2Te_3 is diamagnetic, just as the other pure $A_2^{\mathrm{V}}B_3^{\mathrm{VI}}$ tetradymite semiconductors,[9] and little is known about the magnetic properties upon doping the structure.

In this work, we report on an observation of a ferromagnetic state that sets in at low temperatures when a minute amount of vanadium impurity is introduced into the Sb_2Te_3 matrix. Very recently, a similar material, $Bi_{2-x}Fe_xTe_3$ was identified as a DMS with a ferromagnetic transition temperature of up to 12 K for $x=0.08$.[10] In our structure, which contains a lower concentration of magnetic impurity (vanadium), the magnetic ordering effect appears to be considerably stronger than in the Fe-doped compound. These results bring forth a different semiconducting system that undergoes a ferromagnetic transition at low temperatures and as such broadens the scope of the existing diluted magnetic semiconductors.

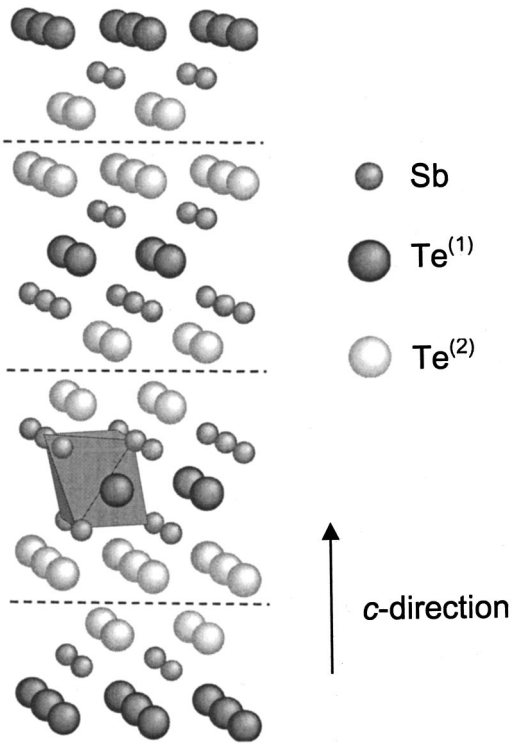

FIG. 1. Atomic layers in the Sb_2Te_3 crystal structure. Dashed lines indicate van der Waals gaps separating five atomic layer lamella. The octahedral coordination is highlighted for a $Te^{(1)}$ atom.

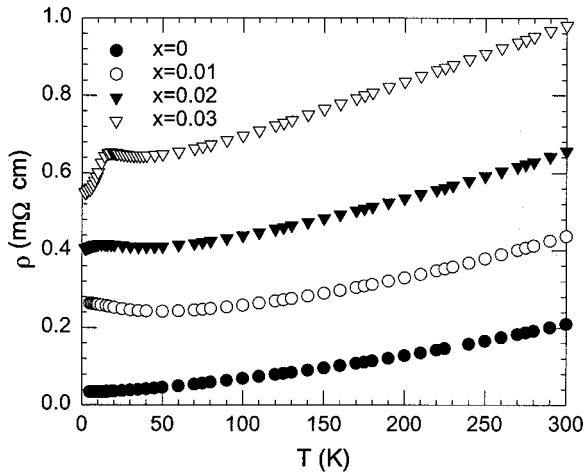

FIG. 2. Temperature dependence of in-plane resistivity for $Sb_{2-x}V_xTe_3$.

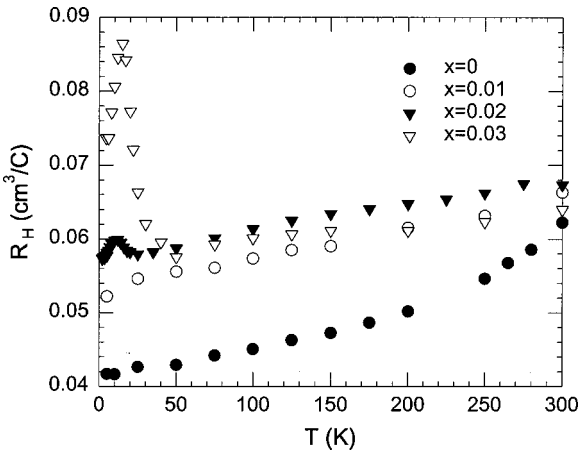

FIG. 3. Temperature dependence of Hall coefficient determined in a field of 10 kG for $Sb_{2-x}V_xTe_3$.

II. EXPERIMENT

Single crystals of $Sb_{2-x}V_xTe_3$ with $x=0$, 0.01, 0.02, 0.03 (nominal) were synthesized using a modified Bridgman method.[11] Bar shaped specimens for transport and magnetic studies were cut with a spark erosion machine to typical dimensions of $1.5\times2.5\times5.5\ mm^3$ where the first dimension is parallel to the *c* axis. Preparation of samples with their long edge parallel to the *c* axis is exceedingly difficult because the structure cleaves very easily along the van der Waals–bonded Te double layers. X-ray lattice parameters were determined from powders with the aid of a Scintag powder diffractometer. Trends in the *c* lattice parameter were also verified using thin single-crystal strata that were cleaved from larger specimens. The results, given in Table I, show that both *a* and *c* decrease monotonically upon addition of vanadium. Analysis of the composition was carried out by both atomic absorption spectroscopy and electron microprobe analysis (EMPA) and actual vanadium concentrations were found to be close to the nominal values. No secondary phases were detected.

Galvanomagnetic measurements were carried out over the temperature range 2–300 K using a low-frequency (16 Hz) a.c. technique. Ohmic contacts to the samples were made with fine copper wires attached with care using a tiny amount of silver paint or indium solder. Magnetic studies were made in a superconducting quantum interference device (SQUID) magnetometer equipped with a 5.5-T superconducting solenoid and the data were corrected for a minor contribution arising from the small plastic sample holder.

III. RESULTS AND DISCUSSION

Anomalies in the low-temperature transport properties of $Sb_{2-x}V_xTe_3$ provided the initial hint of the developing long-range magnetic order. Temperature dependences of the in-plane ($I\perp c$) resistivity ρ and Hall coefficient R_H are shown in Figs. 2 and 3, respectively. Resistivity of the pure Sb_2Te_3 sample increases linearly with temperature over the entire temperature range indicating degenerate Fermi gas carrier transport. The Hall coefficient R_H was obtained in a 10-kG magnetic field oriented parallel to the *c* axis, and is positive with a modest temperature dependence for Sb_2Te_3. The room-temperature carrier (hole) concentration for Sb_2Te_3 is $1.0\times10^{20}\ cm^3$ due to native defects, typical for this compound. Upon addition of vanadium, the resistivity increases but remains metallic, while the values of the carrier concentration change very little. Room-temperature infrared reflectivity measurements in the plasma resonance frequency region (not shown here) corroborate this behavior. The room-

TABLE I. Nominal values of vanadium fraction *x* (with EPMA measured values in parentheses), vanadium concentration N_V, x-ray lattice parameters *a* and *c*, and values of the hole concentration $p=1/eR_H$, resistivity ρ, and Hall mobility μ_H, determined at room temperature.

Nominal *x* (EPMA)	N_V (cm^{-3})	*a* (Å)	*c* (Å)	*p* (cm^{-3})	ρ (mΩ cm)	μ_H (cm^2/V s)
0	0	4.263(1)	30.445(6)	1.0×10^{20}	0.21	297
0.01 (0.010±0.002)	6.3×10^{19}	4.260(8)	30.441(1)	9.4×10^{19}	0.44	152
0.02 (0.016±0.002)	1.0×10^{20}	4.260(3)	30.432(4)	9.3×10^{19}	0.66	103
0.03 (0.026±0.002)	1.6×10^{20}	4.259(0)	30.433(8)	9.8×10^{19}	0.98	65

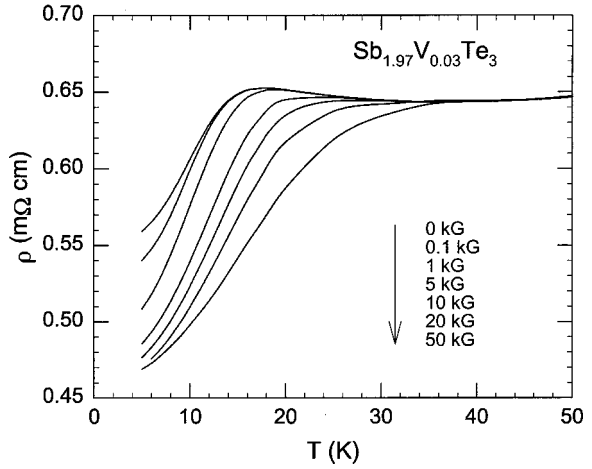

FIG. 4. Temperature dependence of resistivity measured in an increasingly stronger transverse ($B \| c$ axis) magnetic field for $Sb_{1.97}V_{0.03}Te_3$.

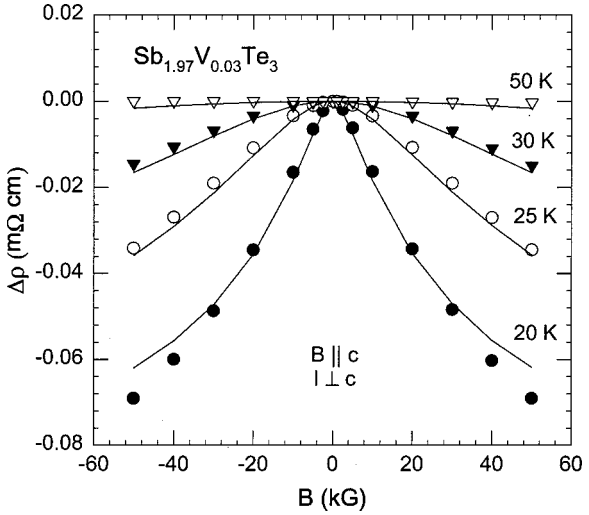

FIG. 5. Field dependence of resistivity at several fixed temperatures near the Curie temperature for $Sb_{1.97}V_{0.03}Te_3$. Solid lines are fits to Eq. (1).

temperature properties are summarized in Table I. Error in the Hall hole concentrations is approximately 5%.

Below 30 K the presence of vanadium leads to a peak in both ρ and R_H that moves to higher temperature as the vanadium content increases. Magnetic semiconductors commonly exhibit a maximum in ρ near their Curie temperature T_C.[12] This critical behavior arises due to scattering of carriers by magnetic spin fluctuations via the exchange interaction. The presence of a magnetic field oriented parallel to the c axis suppresses this peak, as is seen by considering the transverse magnetoresistance data in Fig. 4. Rapid decrease in resistance and large negative magnetoresistance below T_C are a consequence of significantly reduced spin-disorder scattering. Above 50 K, the magnetoresistance is positive, has a parabolic dependence on temperature as is expected from Lorentz force effects, and the magnitude of $\Delta\rho/\rho$ is less than 1% at 50 kG.

Spin-disorder scattering ρ_s can be analyzed by a model proposed by Kasuya,[13] as has been done in other DMS systems [e.g., (Ga, Mn) As (Ref. 14)] which has the form

$$\rho_s = 2\pi^2 \frac{k_F}{pe^2} \frac{m^2 J_{pd}^2}{h^3} N_V [S(S+1) - \langle \mathbf{S} \rangle^2], \tag{1}$$

where k_F is the Fermi wave number, e is the elementary charge, m is the carrier effective mass, h is Planck's constant, N_V and S are the density and spin of vanadium ions, and $\langle \mathbf{S} \rangle$ is the thermal average of $\mathbf{S}$. The p-d exchange term J_{pd} is defined by the interaction Hamiltonian as

$$H = -J_{pd} \sum_i \delta(r - R_i) \mathbf{S}_i \cdot \mathbf{s} \tag{2}$$

where $\mathbf{S}_i$ is the vanadium spin at site R_i and $\mathbf{s}$ is the spin of the carrier at r. The formulation given by Eq. (1) ignores spin-spin correlation of carriers. In Fig. 5 we show the results of the fit to $\Delta\rho = \rho(B) - \rho(0)$ at several temperatures near and above T_C for $Sb_{1.97}V_{0.03}Te_3$. The room-temperature Hall coefficient was used to determine the carrier density p. k_F was calculated from p assuming a spherical Fermi surface. $\langle \mathbf{S} \rangle$ was found directly from the magnetization data using the equation $M = N_V g \mu_B \langle \mathbf{S} \rangle$, where μ_B is the Bohr magneton and $g = 2$ is the Landé g factor. We take $S = 1$ based on the analysis of the magnetization data below. Relying on literature values for the upper valence band hole effective mass of Sb_2Te_3 for a single valley [$m^{\nu} \approx 0.08 m_0$ (Refs. 15 and 16)] which we believe to be appropriate at these low temperatures, and making a correction for the multivalley (sixfold degenerate) nature of the band[17] ($m = 6^{2/3} m^{\nu} = 0.26$), a value for $J_{pd} = 425$ eV Å^3 (or $N_0\beta = 5.3$ eV) is obtained. This J_{pd} value is larger than that for (Ga, Mn)As [3.3 eV (Ref. 14)] when calculated using Eq. (1). A zero field ρ_s of 0.39 mΩ cm is calculated, which seems to be a factor of 2 larger than one would infer from the experimental data in Fig. 4. In either case, spin-disorder scattering appears to be a significant fraction of the total resistivity.

The peak in R_H can be understood by considering the anomalous Hall effect,[18] in which the Hall resistivity ρ_H is expressed as

$$\rho_H = R_0 B + R_s M, \tag{3}$$

where R_0 is the ordinary Hall coefficient, R_s the anomalous Hall coefficient, and M the magnetization of the samples. For temperatures above T_C, ρ_H is linear in magnetic field up to $B = 50$ kG with zero intercept implying that the second term in Eq. (3) is insignificant in this temperature range. Below T_C, the transition to the ferromagnetic phase results in a large M and thus the second term becomes significant. The maximum in R_H seen in Fig. 3 results from a peak in R_s that occurs at a temperature close to T_C in ferromagnetic materials.[18]

To verify the presence of the magnetic order, we carried out detailed magnetic measurements with the aid of a SQUID magnetometer. Magnetic susceptibility χ versus temperature obtained by cooling in a field of 1 kG oriented parallel to the c axis of the samples is shown in Fig. 6. A value of $\chi = -3.8 \times 10^{-7}$ emu/g, roughly independent of tempera-

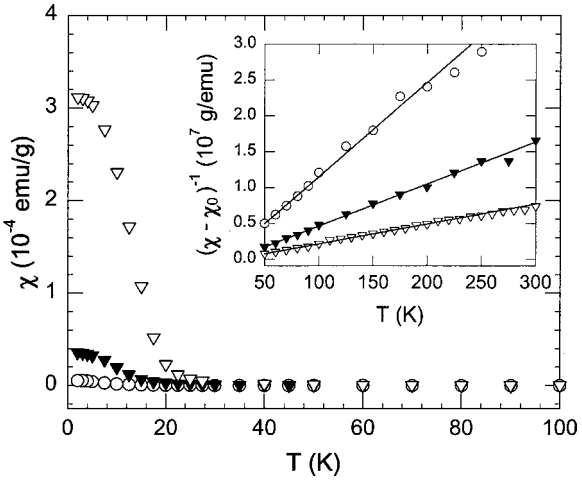

FIG. 6. Magnetic susceptibility versus temperature for $Sb_{2-x}V_xTe_3$ with $x=0.01$ (open circles), $x=0.02$ (filled triangles), and $x=0.03$ (open triangles). The inset shows the experimental data together with a fit to a Curie-Weiss law [Eq. (4)]. The fitting parameters are given in Table II.

ture, was found for Sb_2Te_3 confirming the diamagnetic nature of pure $A_2^{\mathrm{V}}B_3^{\mathrm{VI}}$ tetradymite semiconductors. The transition to the ferromagnetic state for the samples containing vanadium is very clear as χ becomes positive and very large below T_C. Above the magnetic transition temperature, the magnetic susceptibility is well described by a Curie-Weiss law,

$$\chi = \frac{C}{T-\Theta_p} + \chi_0, \tag{4}$$

where C is the Curie constant, Θ_p is the paramagnetic Curie temperature, and χ_0 is the temperature independent diamagnetic lattice term. The fits to the data using Eq. (4) are shown in the inset of Fig. 6 and the fitting parameters are given in Table II. For a given concentration of vanadium in each sample, the magnetic state of the ions can be inferred from the Curie constant using the equation $C=N_V\mu_B^2 p_{\mathrm{eff}}^2/3k_B$. Here, N_V is the concentration of vanadium atoms, μ_B is the Bohr magneton, p_{eff} is the effective Bohr magneton number given by $g[S(S+1)]^{1/2}$ with the Landé g factor ($g=2$) and the spin S. We are assuming complete quenching of the orbital angular momentum, which is the usual case for transition-metal ions. We note that the values of p_{eff} increase from 1.9 to 2.6 as x increases from 0.01 to 0.03. This might indicate an evolution to a predominantly 3+ valence state of vanadium (expected spin only value of $p_{\mathrm{eff}}=2.83$). We caution, however, that the very low concentrations of vanadium in these samples lead to uncertainty in the determination of x and hence p_{eff}. Detailed electron spectroscopy studies would shed more light on this issue.

The magnetization behavior of the structure is shown in Fig. 7. The wide hysteresis loops observed when the field is oriented parallel to the c axis [Fig. 7(a)] are an unambiguous signature of ferromagnetic ordering in these samples. Although not obvious from the plot, the $x=0.01$ sample shows hysteresis with a small coercive field of approximately 250 G. Such smooth hysteresis loops (no apparent discontinuities) are suggestive of coherent rotation[19] of spins in this system. Another estimate of the spin of the vanadium ions can be obtained using the equation $M_{\mathrm{sat}}=N_V g\mu_B S$ and the results are given in Table II. Again we see a similar trend in the effective Bohr magneton numbers as the vanadium content increases. When the magnetic field is applied perpendicular to the c axis as shown in Fig. 7(b) practically no hysteresis is detected indicating that the easy axis for magnetization is parallel to the c axis. This may reflect the anisotropic structure of the tetradymite semiconductors.

Perhaps the most spectacular revelation of the long-range magnetic order in the transport data comes from the hysteretic behavior in the transverse magnetoresistance ($B\|c$ axis and current $\perp c$ axis) displayed in Fig. 7(c). The large and sharp maxima on the magnetoresistance curve occur at magnetic fields that correspond to zero magnetization (coercive field) and therefore maximum spin disorder in the system. One-half of the width between the maxima matches very well the coercive field values obtained from hysteresis in the magnetization loops. Anisotropy of this system was further probed by investigating the magnetoresistance as a function of the angle between the applied magnetic field and the crystallographic orientation. Figure 8 depicts this data normalized to the $B\|c$ ($\theta=90°$) value taken at several temperatures for the $x=0.03$ sample. Below T_C, a maximum in $R/R_{B\|c}$ develops and grows with decreasing temperature. As temperature decreases, the peak is first symmetric and its position corresponds to the $B\perp c$ orientation, but becomes asymmetric and begins to shift to higher angles below 10 K. The data shown are taken in increasing θ. For data taken in decreasing θ, the peak positions at low temperatures again occur after B crosses the c plane (now at negative θ), i.e., hysteresis is observed.

TABLE II. Parameters from the fit of the magnetic susceptibility data to the Curie-Weiss law [Eq. (4)]. Also given are Curie temperatures T_c, determined from Arrott plots, together with effective Bohr magneton numbers per vanadium ion obtained from the Curie constant $p_{\mathrm{eff}}^{(1)}$ and from the saturation value of the magnetization at 2 K, $p_{\mathrm{eff}}^{(2)}$.

x	C [emu K/g]	χ_0 [emu/g]	Θ_p [K]	T_c [K]	$p_{\mathrm{eff}}^{(1)}$ V	$p_{\mathrm{eff}}^{(2)}$ V
0.01	7.610×10^{-6}	-4.03×10^{-7}	12.5	11	1.9	1.5
0.2	1.705×10^{-5}	-4.21×10^{-7}	21.2	17	2.3	2.1
0.03	3.598×10^{-5}	-4.72×10^{-7}	23.4	22	2.6	2.3

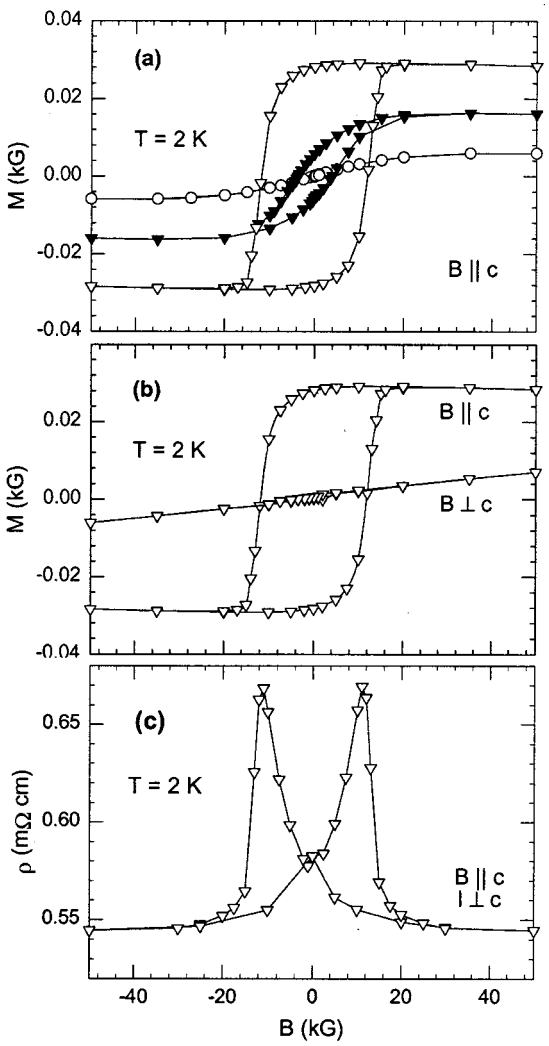

FIG. 7. Field dependence of the magnetization measured at 2 K for $Sb_{2-x}V_xTe_3$ with $x=0.01$ (open circles), $x=0.02$ (filled triangles), and $x=0.03$ (open triangles). In (a), the field is aligned parallel to the c axis. In (b), data for $x=0.03$ is shown for field aligned both parallel and perpendicular to the c axis indicating that the c axis is the easy axis for magnetization. In (c), the magnetoresistance displays hysteresis corresponding to the magnetization data.

The temperature dependence of the coercive field H_c for $Sb_{2-x}V_xTe_3$ is shown in Fig. 9. We compare the magnetization values of H_c for $x=0.03$ to the positions of the peaks in the hysteretic pattern of low-temperature magnetoresistance ("+" symbols in Fig. 9). It is found that the hysteretic behavior of both magnetization and transport measurements agree with each other. This correspondence is not surprising since, as the sample becomes demagnetized at H_c, the scattering of carriers increases due to spin disorder scattering. This interpretation is also consistent with the angular dependence of the magnetoresistance. The crystal anisotropy may contribute to this effect since the spins clearly only tend to orient themselves along the c axis as evidenced by Fig. 7.

Magnetic-field dependence of the magnetization for $Sb_{2-x}V_xTe_3$ was investigated over a broad temperature region. In the case of a conventional second-order ferromagnetic transition, Arrott plots should give positive slope straight lines given that the magnetic field is high enough so that possible domain or stray field effects are not seen. In these materials, the saturation field at low temperature is near 25 kG as is seen in Fig. 7(a). Indeed, for fields below 25 kG and especially below the ordering temperature, we see deviation from linear behavior. However, from the high-field extrapolation of the data, we were able to make an estimate of the temperature dependence of the spontaneous magnetization M_s and the Curie temperature T_C. This data are shown in Fig. 10. The inset to Fig. 10 indicates that near T_C, the curves are parallel and evenly spaced with temperature. From the slight curvature at these fields (30–55 kG), one can see that the Curie temperatures estimated here are the lower limits. Arrott plots for $x=0.01$ displayed strong curvature at low temperatures which made it difficult to determine M_s versus T much below T_C, thus we only show $x=0.02$ and

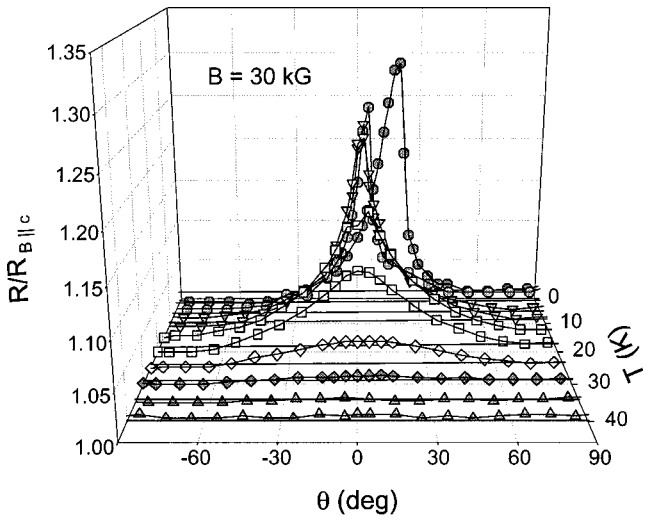

FIG. 8. Transverse magnetoresistance as a function of angle between the applied magnetic field and the c plane of $Sb_{1.97}V_{0.03}Te_3$ at several temperatures. Here $\theta=0°$ corresponds to $B\perp c$.

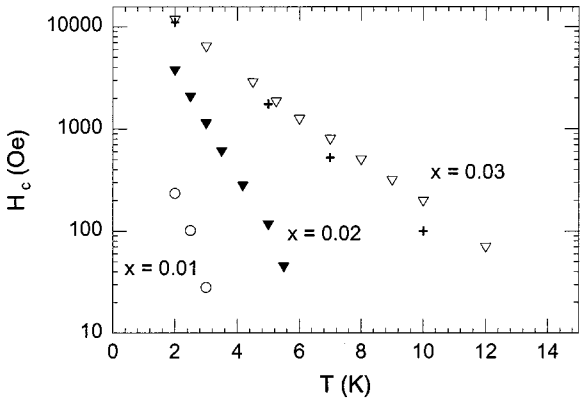

FIG. 9. Temperature dependence of the coercive field determined from magnetization hysteresis loops of $Sb_{2-x}V_xTe_3$ (open and closed symbols). "+" symbols designate peak positions in magnetoresistance obtained from hysteresis measurements (see Fig. 7). A direct correspondence between magnetization and magnetoresistance is apparent.

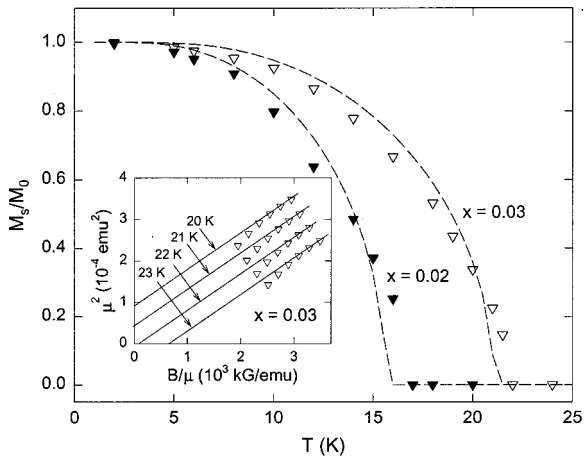

FIG. 10. Saturation magnetization versus temperature for $Sb_{2-x}V_xTe_3$ with $x=0.02$ and 0.03. Dotted lines are predictions according to mean-field theory taking $S=1$. The inset is an Arrott plot for $x=0.03$ at several temperatures near the Curie temperature and the solid lines are high-field extrapolations of the data.

0.03 here. The dashed lines in Fig. 10 are predictions based on mean field theory with $S=1$.

An important step toward understanding the ferromagnetic state in these structures is to ascertain the location of the vanadium ions in the Sb_2Te_3 host lattice. Impurity atoms can be incorporated into the Sb_2Te_3 crystal lattice by substituting for the cation (Sb) or anion (Te), by occupying interstitial lattice sites, or possibly by entering the van der Waals gaps. We offer the following scenario concerning the position of vanadium in the lattice. The ionic radii of Sb^{3+} and Te^{2-} in the octahedral coordination of the tetradymite structure are 0.90 and 2.07 Å, respectively. This is to be compared to the ionic radii of various vanadium ions. Vanadium ($3d^34s^2$) can give up its $4s$ electrons to become V^{2+} (with an ionic radius of 0.93 Å in octahedral coordination). Alternatively, vanadium can assume $3+(0.78\ \text{Å})$, $4+(0.72\ \text{Å})$, or even $5+(0.50\ \text{Å})$ configurations.[20] The above size considerations suggest that vanadium of any valence state is far more likely to substitute for Sb than for Te. If vanadium entered into the lattice in interstitial positions or the van der Waals gap, i.e., not forming strong bonds, it would likely lose its electrons to the conduction band, thus behaving as an effective electron donor. This situation is not supported by the experimental evidence that indicates substantial insensitivity of the carrier concentration to the actual vanadium content. Furthermore, one would expect the c lattice parameter to increase rather than decrease if vanadium were in the van der Waals gap. Taken together with the values of p_{eff}, the data suggest that the most likely scenario is vanadium substitution on the Sb sublattice in the V^{3+} valence state that saturates bonding and exactly matches the valence state of Sb in the structure.

Magnetic properties of diluted magnetic semiconductors have been explained by various physical mechanisms depending on the concentrations of magnetic ions and free carriers. For Mn-based II-VI DMS's where the transition-metal ion concentration is high and carrier concentration low, the dominant interaction is antiferromagnetic due to the superexchange interaction.[2] In III-V DMS's, the maximum Mn concentration is lower (up to ~7% using low-temperature MBE techniques); however, in the presence of a high hole density, a carrier mediated ferromagnetic interaction is invoked which has been discussed within a number of frameworks including the Ruderman-Kittel-Kasuya-Yosida (RKKY) interaction[21] and a mean-field theory.[22] The Zener model description,[23] a variant approach, implies that the Curie temperature T_C is determined by a competition between the ferromagnetic and antiferromagnetic interactions, and predicts that T_C increases with hole concentration. In our samples with very dilute content of vanadium and large carrier (hole) background, a likely scenario for the onset of the ferromagnetic state is the RKKY interaction. However, we cannot rule out alternative theories which challenge the free-carrier based explanation of the ferromagnetism.[24–26] We wish to note that the less than half filled d shell reflecting the magnetic state of vanadium is unusual in the context of diluted magnetic semiconductors. It has been proposed[27] that under these conditions the superexchange among the magnetic ions is ferromagnetic rather than antiferromagnetic. The fact that the magnetoresistance can be described well within the Kasuya theory lends support to the RKKY interaction mediated by holes for the origin of the ferromagnetism, though further study is needed to elucidate the mechanism.

IV. SUMMARY

In summary, a diluted magnetic semiconductor based on the layered, narrow-band-gap Sb_2Te_3 doped with vanadium was discovered. Magnetization studies reveal that the easy axis for magnetization lies along the c axis. The sample with composition $Sb_{1.97}V_{0.03}Te_3$ has a hole concentration of $9.8\times10^{19}\ \text{cm}^{-3}$ and a Curie temperature of at least 22 K. Through an effort to incorporate more vanadium ions into the Sb_2Te_3 structure and the use of known effective acceptors,[28] there are excellent prospects for achieving higher Curie temperatures via increased densities of both holes and magnetic ions. Existing methods [including MBE (Refs. 29 and 30)] for thin-film growth of Sb_2Te_3 and related tetradymite structures may help to explore the upper limit of magnetic ion incorporation. These tetradymite-based materials are not in the mainstream of present-day semiconductor technology and interfacing these materials with current thin-film device applications poses a challenge. Nevertheless, one ought to investigate the full scope of the physical properties and new science that the structure might support. We stress that in our system, we move away from the usual environment of a zinc-blende crystal structure and Mn ions that underpin the magnetic properties of the existing DMS's. Therefore these results pave the way for a new parameter space for search and exploration of other diluted magnetic semiconductors based on the $A_2^{\text{V}}B_3^{\text{VI}}$ tetradymite system doped with $3d$ transition elements.

ACKNOWLEDGMENTS

We gratefully acknowledge research support provided by NATO grant HTECH CRG 873186, and by DARPA contract N0014-98-3-0011.

*Author to whom correspondence should be addressed. Email address: cuher@umich.edu

[1] T. Kasuya and A. Yanase, Rev. Mod. Phys. **40**, 684 (1968).
[2] *Diluted Magnetic Semiconductors*, Semiconductors and Semimetals Vol. 25, edited by J. K. Furdyna and J. Kossut (Academic, London, 1988).
[3] H. Munekata, H. Ohto, S. von Molnár, A. Segmüller, L. L. Chang, and L. Esaki, Phys. Rev. Lett. **63**, 1849 (1989).
[4] H. Ohno, H. Munekata, T. Penney, S. von Molnár, and L. L. Chang, Phys. Rev. Lett. **68**, 2664 (1992).
[5] H. Ohno, A. Shen, F. Matsukura, A. Oiwa, A. Endo, S. Katsumoto, and Y. Iye, Appl. Phys. Lett. **69**, 363 (1996).
[6] H. Scherrer and S. Scherrer, in *CRC Handbook of Thermoelectrics*, edited by D. M. Rowe (Chemical Rubber, Boca Raton, FL, 1995), p. 211.
[7] See, e.g., H. J. Goldsmid, *Electronic Refrigeration* (Pion Limited, London, 1986).
[8] H. T. Langhammer, M. Stordeur, H. Sobotta, and V. Riede, Phys. Status Solidi B **109**, 673 (1982).
[9] J. Horák, M. Matyáš, and L. Tichý, Phys. Status Solidi A **27**, 621 (1975).
[10] V. A. Kul'bachinskiĭ, A. Y. Kaminskii, K. Kindo, Y. Narumi, K. Suga, P. Lošťák, P. Svanda, Pis'ma Zh. Eksp. Teor. Fiz. **73**, 396 (2001) [JETP Lett. **73**, 352 (2001)].
[11] P. Lošťák, L. Beneš, S. Civiš, and H. Süssmann, J. Mater. Sci. **25**, 277 (1990).
[12] S. von Molnár and T. Kasuya, Phys. Rev. Lett. **21**, 1757 (1968).
[13] T. Kasuya, Prog. Theor. Phys. **16**, 45 (1956).
[14] F. Matsukura, H. Ohno, A. Shen, and Y. Sugawara, Phys. Rev. B **57**, R2037 (1998).
[15] B. Roy, B. R. Chakraborty, R. Bhattacharya, and A. K. Dutta, Solid State Commun. **25**, 617 (1978).
[16] V. A. Kulbachinskii, N. Miura, H. Arimoto, T. Ikaida, P. Lošťák, H. Horák, and C. Drašar, J. Phys. Soc. Jpn. **68**, 3328 (1999).
[17] M. Stordeur, in *CRC Handbook of Thermoelectrics* (Ref. 6), p. 239.
[18] C. M. Hurd, *The Hall Effect in Metals and Alloys* (Plenum, New York, 1972), p. 153.
[19] E. C. Stoner and E. P. Wohlfarth, Philos. Trans. R. Soc. London, Ser. A **240**, 599 (1948).
[20] R. D. Shannon, Acta Crystallogr., Sect. A: Cryst. Phys., Diffr., Theor. Gen. Crystallogr. **32**, 751 (1976).
[21] T. Story, R. R. Galazka, R. B. Frankel, and P. A. Wolff, Phys. Rev. Lett. **56**, 777 (1986).
[22] T. Dietl, A. Haury, and Y. Merle d'Aubigné, Phys. Rev. B **55**, R3347 (1997).
[23] T. Dietl, H. Ohno, F. Matsukara, J. Cibert, and D. Ferrand, Science **287**, 1019 (2000).
[24] H. Akai, Phys. Rev. Lett. **81**, 3002 (1998).
[25] T. Ogawa, M. Shirai, N. Suzuki, and I. Kitagawa, J. Magn. Magn. Mater. **196–197**, 428 (1999).
[26] V. I. Litvinov and V. K. Dugaev, Phys. Rev. Lett. **86**, 5593 (2001).
[27] J. Blinowski and P. Kacman, Phys. Rev. B **46**, 12298 (1992).
[28] J. Navrátil, I. Klichová, S. Karamazov, J. Srámková, and J. Horák, J. Solid State Chem. **140**, 29 (1998).
[29] A. Mzerd, D. Sayah, J. C. Tedenac, and A. Boyer, J. Cryst. Growth **140**, 365 (1994).
[30] Y. Iwata, H. Kobayashi, S. Kikuchi, E. Hatta, and K. Mukasa, J. Cryst. Growth **203**, 125 (1999).